

1 Impact of salinity on element incorporation in two 2 benthic foraminiferal species with contrasting 3 Magnesium contents

4 Esmee Geerken¹, Lennart Jan de Nooijer¹, Inge van Dijk^{1,2} & Gert-Jan Reichart^{1,3}

5 ¹Department of Ocean Systems, NIOZ-Royal Netherlands Institute for Sea Research, and Utrecht
6 University, Den Burg, The Netherlands

7 ²Currently at: UMR CNRS 6112 LPG-BIAF, University of Angers, France

8 ³Faculty of Geosciences, Utrecht University, Utrecht, The Netherlands

9 *Correspondence to:* Esmee Geerken (esmee.geerken@nioz.nl)

10 **Abstract.** Accurate reconstructions of seawater salinity could provide valuable constraints for studying
11 past ocean circulation, the hydrological cycle and sea level change. Controlled growth experiments and
12 field studies have shown the potential of foraminiferal Na/Ca as a direct salinity proxy. Incorporation
13 of minor and trace elements in foraminiferal shell carbonate varies, however, greatly between species
14 and hence extrapolating calibrations to other species needs validation by additional (culturing) studies.
15 Salinity is also known to impact other foraminiferal carbonate-based proxies, such as Mg/Ca for
16 temperature and Sr/Ca for sea water carbonate chemistry. Better constraints on the role of salinity on
17 these proxies will therefore improve their reliability. Using a controlled growth experiment spanning a
18 salinity range of 20 units and analysis of element composition on single chambers using laser ablation-
19 Q-ICP-MS, we here show that Na/Ca correlates positively with salinity in two benthic foraminiferal
20 species (*Ammonia tepida* and *Amphistegina lessonii*). The Na/Ca values differ between the two species,
21 with an approximately 2-fold higher Na/Ca in *A. lessonii* than in *A. tepida*, coinciding with an offset in
22 their Mg content (~35 mmol/mol versus ~2.5 mmol/mol for *A. lessonii* and *A. tepida*, respectively).
23 Despite the offset in average Na/Ca values, the slopes of the Na/Ca-salinity regressions are similar
24 between these two species (0.077 versus 0.064 mmol/mol change per salinity unit). In addition, Mg/Ca
25 and Sr/Ca are positively correlated with salinity in cultured *A. tepida*, but show no correlation with
26 salinity for *A. lessonii*. Electron microprobe mapping of incorporated Na and Mg of the cultured
27 specimens shows that within chamber walls of *A. lessonii*, Na/Ca and Mg/Ca occur in elevated bands in
28 close proximity to the primary organic lining. Between species, Mg-banding is relatively similar, albeit
29 that Mg content is 10 times lower and that variation within the chamber wall is much less pronounced
30 in *A. tepida*. In addition, Na-banding is much less prominent in this species than it is in *A. lessonii*.
31 Inter-species differences in element banding reported here are hypothesized to be caused by differences
32 in biomineralization controls responsible for element uptake.

33 **1. Introduction**

34 Sea water salinity varies over time and space as a function of continental ice volume, evaporation,
35 precipitation and river runoff. Salinity reconstructions could provide important constraints on past
36 ocean circulation, the hydrological cycle and glacial-interglacial sea level changes. Currently, most
37 reconstructions of salinity are indirect and based on the correlation between salinity and $\delta^{18}\text{O}_{\text{water}}$,
38 assuming this relationship to be constant over space and time (Rohling and Bigg, 1998). An
39 independent salinity proxy may reduce the uncertainties inherently associated with such approaches
40 (Rohling and Hilgen, 2007) and should preferably be based on one of the main components of sea
41 water salinity, for instance sodium (Na). Results from a culture study showed that the sodium content
42 of foraminiferal calcite ($\text{Na}/\text{Ca}_{\text{cc}}$) correlates positively and linearly with salinity for the benthic low-
43 Mg, symbiont-barren species *Ammonia tepida*, with a sensitivity of 0.22 mmol/mol for every change of
44 1 salinity unit between salinities 30 and 38.6 (Wit et al., 2013). Various culture studies earlier showed
45 that also Mg/Ca is affected by salinity, but responds more strongly to changes in temperature (Lea et
46 al., 1999; Dissard et al., 2010b; Nürnberg et al., 1996; Hönisch et al., 2013). Although an effect of
47 salinity on foraminiferal Sr/Ca_{cc} has been reported in some studies (Kırsakürek et al., 2008; Dissard et
48 al., 2010b; Wit et al., 2013) other studies did not find a relation between salinity and foraminiferal
49 Sr/Ca (Dueñas-Bohórquez et al., 2009; Diz et al., 2012; Allen et al., 2016), which lead to the
50 hypothesis that foraminiferal Sr/Ca mainly reflects sea water inorganic carbon chemistry (Keul et al.,
51 2017) in addition to its response to temperature (Lea et al., 1999; Raja et al., 2007). Hence, an
52 independent salinity proxy would not only be useful for constraining past (changes in) salinity, but also
53 improve temperature reconstructions based on Mg/Ca_{cc} and reconstructions of past sea water carbonate
54 chemistry based on Sr/Ca.

55 Following the culture-based Na/Ca_{cc}-salinity calibration for *A. tepida* (Wit et al., 2013), a culture study
56 with planktonic symbiont-bearing species also showed a significant linear relationship for
57 *Globigerinoides ruber* (Allen et al., 2016). Although no significant relationship was observed in this
58 study for *G. sacculifer* (Allen et al., 2016), a recent field calibration observed positive linear
59 relationships for both these species (Mezger et al., 2016). Still, the Na/Ca-salinity sensitivities observed
60 between the different species and studies differed considerably (ranging from a change in 0.074 to 0.66
61 mmol/mol in Na/Ca_{cc} for a change in 1 salinity unit). Whereas Wit et al. (2013) suggested an
62 incorporation mechanism similar to that observed in inorganic calcite, field and culture studies also
63 show that different species of foraminifera have varying calcite chemistries, thereby resulting in the
64 need of species-specific calibrations similar to many other foraminiferal trace metal-based proxies (e.g.
65 Elderfield and Ganssen, 2000; Rosenthal et al., 2000; Anand et al., 2003; Bemis et al., 1998; Toyofuku
66 et al., 2011). For example, Mg/Ca_{cc} values are different between groups of low-Mg-, high-Mg hyaline
67 and porcelaneous foraminifera (Toyofuku et al., 2000; Segev and Erez, 2006; Raja et al., 2007), which
68 also seems to be reflected in other co-precipitated cations (De Nooijer et al., 2017). Hence, calibration
69 of Na/Ca_{cc} as a function of salinity for other species is not only necessary to test the applicability of this
70 novel proxy for other groups of foraminifera, but also allows testing whether monovalent cations
71 follow the inter-species trends described for divalent cations (Terakado et al., 2010).

72 Here we calibrated Na-, Mg- and Sr-incorporation in the intermediate-Mg calcite benthic foraminiferal
 73 species *Amphistegina lessonii* and the low-Mg calcite species *Ammonia tepida* over a salinity range of
 74 20 units (from 25 to 45). We thus compare the El/Ca versus salinity trends in a tropical, symbiont-
 75 bearing species (*A. lessonii*) to a temperate intertidal symbiont-barren species (*A. tepida*) and both of
 76 them to existing calibrations. The chemical composition of newly formed calcite was determined by
 77 Laser Ablation Inductively Coupled Plasma Mass Spectrometry (LA-Q-ICP-MS), providing insights in
 78 concentrations and variability therein between specimens and between single chambers. To investigate
 79 intra-specimen variability at the scale of the chamber wall we also performed Electron Probe Micro
 80 Analysis (EPMA), mapping the Ca, Na and Mg distribution throughout the chamber wall for specimens
 81 of both species cultured.

82 2. Methods

83 2.1 Culture media preparation and chemistry

84 In total, 50 L of sea water with a salinity of 50 was prepared by sub-boiling 0.2 μm filtered North
 85 Atlantic sea water for 48 hours at 45 °C. Subsequently, culture media were obtained by diluting this
 86 high-saline sea water with double de-ionized sea water (~18 M Ω) in batches of approximately 10L
 87 with salinity increasing from 25 to 45 in steps of 5 units, resulting in 5 unique salinity conditions.
 88 Using a single batch of concentrated sea water to subsequently dilute to the desired salinities ensures
 89 constant element to Ca ratios. Salinity of the media was measured with a salinometer (VWR CO310),
 90 based on conductivity. Culture media were stored in Nalgene containers and kept in the dark at 10 °C.
 91 Sea water pH was determined with a pH meter (pH110, VWR). Subsamples were taken prior to and at
 92 the end of the experiment and analyzed for DIC and element concentrations to monitor the effect of
 93 sub-boiling on the sea water's inorganic carbon chemistry and element composition (Table 1).
 94 Subsamples for DIC were collected in headspace-free vials and conserved with a saturated HgCl₂
 95 solution (10 μl HgCl₂/10 ml sample). DIC measurements were performed on an autoanalyzer
 96 spectrometric system TRAACS 800; Stoll et al. (2001). This analysis requires only a small amount of
 97 sample, while yielding high accuracy ($\pm 2 \mu\text{mol/kg}$) and precision ($\pm 1.5 \mu\text{mol/kg}$). The minor and major
 98 elemental composition of the culture media was measured using a sector field ICP-MS (Element2,
 99 Thermo Scientific) by sampling 1 ml from the culture media and dilution by a factor 300 with 0.14 M
 100 HNO₃ (Table 1).

101 **Table 1.** Experiment culture media measurements per salinity condition. Carbonate ion concentrations
 102 and saturation state with respect to calcite (at 25 °C) were calculated using CO2SYS (Van Heuven et
 103 al., 2011) and the equilibrium constants K1 and K2 of Mehrbach et al. (1973), as reformulated by
 104 (Dickson and Millero, 1987).

Experiment	Na/Ca _{sw} mol/mol	Mg/Ca _{sw} mol/mol	Sr/Ca _{sw} mmol/mol	Salinity	DIC $\mu\text{mol/kg}$	pH	[CO ₃ ²⁻] mmol/kgSW	Ω_{calcite}
S25	48.84	5.61	9.37	25.2	1087.3	8.32	164.90	4.28
S30	49.79	5.69	9.45	30.3	1305.3	8.28	205.98	5.15
S35	48.56	5.51	9.04	35.2	1512.0	8.22	258.84	6.22
S40	48.50	5.62	9.19	40.0	1734.4	8.17	267.23	6.16

S45	48.90	5.73	9.21	45.2	1947.4	8.10	284.67	6.23
------------	-------	------	------	------	--------	------	--------	------

105

106 **2.2 Collection of foraminifera and culture set-up**

107 Surface sediment samples containing foraminifera (*A. lessonii*) were collected from the Indo-Pacific
108 Coral Reef aquarium in Burgers' Zoo (Arnhem, The Netherlands; Ernst et al., 2011) and a tidal flat
109 near Den Oever, the Wadden Sea (*A. tepida*, genotype T6; Hayward et al., 2004). Sediment was stored
110 in aerated aquaria at 25°C (*A. lessonii*) and 10°C (*A. tepida*) with a day/night cycle of 12/12 hours,
111 similar to conditions in the coral reef aquarium and Wadden Sea, respectively. From both stocks, living
112 specimens, recognized by chambers that were filled with yellow cytoplasm and pseudopodial activity,
113 were isolated.

114 The culture protocol was the same for both species to facilitate comparison of obtained Element/Ca
115 ratios between species. Since our specimens of *A. tepida* are from a location with a much larger
116 temperature range than where *A. lessonii* is derived from (Ernst et al., 2011; Van Aken, 2008; De
117 Nooijer et al., 2014a), both species were incubated at 25 °C. Living specimens were placed in groups of
118 25 individuals in Petri dishes with approximately 70 ml of North Atlantic surface sea water (0.2 µm
119 filtered) and fed with fresh cells of the algae *Dunaliella salina*. After reproduction, which occurred in
120 approximately 2/3 of all incubated specimens in both species, 2-3 chambered juveniles were isolated.
121 The use of specimens from reproduction events guarantees that virtually all chambers present at the end
122 of the experiment were produced under the culture conditions (De Nooijer et al., 2014a). Strains of
123 specimens of the reproduction events were divided over Petri dishes (resulting in 2-10 individuals per
124 dish) with approximately 10 ml culture medium and stored in a temperature controlled incubator set at
125 25 °C with a day/night cycle of 12/12 hours. The culture media in the Petri dishes were replaced once
126 every week, after which specimens were fed with 1 ml concentrated and freeze-dried *Dunaliella salina*
127 diluted with the culture medium for each salinity condition, to minimize changes in salinity when
128 feeding the foraminifers. The amount of food was adjusted so that it was not depleted after a week, at
129 the same time not resulting in an excess of debris and hence reduce bacterial growth. Petri dishes were
130 sealed with a lid to minimize evaporation. After 6-8 weeks, specimens were harvested and transferred
131 to microvials to clean the specimens' carbonate shells from cell material. Specimens were cleaned with
132 an adapted version of the Barker protocol (Barker et al., 2003), only applying the organic removal /
133 oxidation step, in which NaOH was replaced with NH₄OH, in order to avoid Na-contamination of our
134 samples. Organic matter was removed by adding 1% H₂O₂ buffered with 0.1M NH₄OH at 90 °C and
135 gentle ultrasonication (80kHz, 50% power, in degas mode) for 1 min, which is known not to affect
136 obtained Mg/Ca and Sr/Ca (Barker et al., 2003). Specimens were subsequently rinsed 3 times with
137 double de-ionized water, dried in a laminar flow cabinet, after which their size was determined (i.e. the
138 maximum diameter crossing the centre of the specimen). The specimens were thereafter stored until
139 geochemical analyses (LA-Q-ICP-MS; 2.2.2 and EPMA; 2.4).

140 **2.2.2 Foraminiferal calcite chemistry**

141 Specimens were fixed on a laser ablation-stub using double sided tape, carefully positioning them to
 142 allow ablation of the last chambers (Appendix A). Element concentrations of individual chambers were
 143 measured with LA-ICP-MS (Reichert et al., 2003). The last 1-3 chambers of each specimen were
 144 ablated using a circular spot with a diameter of 60 μm (*A. tepida*) and 80 μm (*A. lessonii*)
 145 (NWR193UC, New Wave Research) in a helium environment in a New Wave TV2 dual-volume cell
 146 (cup volume of $\sim 1\text{ cm}^3$) at a repetition rate of 6 Hz and an energy density of approximately 1 J/cm².
 147 The aerosol was transported to a quadrupole ICP-MS (iCap, Thermo Scientific) on a helium flow at a
 148 rate of 0.7 L/min, with 0.4 L/min Argon make-up gas being added before entering the torch. Nitrogen
 149 gas was added at a rate of 5 ml/ minute to enhance sensitivity of the analysis. Before entering the torch,
 150 the aerosol/ Ar/ He mixture passed through an in-house made smoothing device to reduce temporal
 151 variations in signal strength. Monitored masses included ⁷Li, ¹¹B, ²³Na, ²⁴Mg, ²⁵Mg, ²⁷Al, ⁴³Ca, ⁴⁴Ca,
 152 ⁶⁰Ni, ⁶⁶Zn, ⁸⁸Sr, ¹³⁷Ba and ²³⁸U, with one full cycle through the different masses taking 120 ms.
 153 Calibration was performed against a MACS-3 (synthetic calcium carbonate) pressed powder carbonate
 154 standard with ⁴³Ca as an internal standard. Count rates for the different masses were directly translated
 155 into element/Ca_{cc} (El/Ca_{cc}) ratios. Internal precision based on MACS-3 is 4% for Na, 3% for Mg and
 156 4% for Sr. Accuracy and relative analytical errors, based on measuring international standards JCp-1
 157 coral (*Porites* sp.) powder and the NIST (National Institute of Standards and Technology) SRM 610
 158 and SRM 612 (glass) are listed in Table 2. The relatively large offset between the glass standards and
 159 the pressed powders (both MACS-3 and JCp-1) is known not to influence obtained El/Ca_{cc} ratios when
 160 either one is used as calibration standard (Hathorne et al., 2008), but due to the similar matrix, MACS-
 161 3 was chosen as calibration standard.

162 **Table 2.** Accuracies (Ac) and precisions (Pr) for Na, Mg and Sr for the various standards analyzed.

Standard	n	Ac Na (%)	Pr Na (%)	Ac Mg (%)	Pr Mg (%)	Ac Sr (%)	Pr Sr (%)
JCp-1	51	99	6	96	6	96	4
NIST610	32	119	3	104	2	110	3
NIST612	29	119	3	104	2	110	2

163
 164 In total, 675 chambers were measured (336 for *Amphistegina* and 339 for *Ammonia*), resulting in
 165 between 52 to 125 single chamber measurements per salinity condition per species. These
 166 measurements were done on the last three (final or F, penultimate or F-1 and pre-penultimate or F-2)
 167 chambers of these specimens (see Table 3 for number of specimens and average number of spots per
 168 specimen). Element concentrations were calculated from the time (i.e. ablation depth) resolved profiles
 169 using an adapted version of the SILLS (Signal Integration for Laboratory Laser Systems; Guillong et
 170 al., 2008)) package for MATLAB (for details see Van Dijk et al., 2017a), while taking care to exclude
 171 contaminations potentially present on chamber walls (examples of profile selection: Dueñas-Bohórquez
 172 et al., 2011; Wit et al., 2013; Mewes et al., 2014; Mezger et al., 2016; Van Dijk et al., 2017b).
 173 Measurements with ablation yields or integrations times <5 s were excluded from further analysis.
 174 The LA measurements were also used to investigate the co-occurrence of elements within specimens.
 175 Since there is variability in Ca counts between the laser ablation measurements, single-spot based

176 Element/Ca_{cc} ratios may cause spurious correlation due to coupled differences in Ca counts. To test
177 whether observed correlations between Na/Ca_{cc}, Sr/Ca_{cc} and Mg/Ca_{cc}, based on single-spots, are due to
178 the use of a common denominator (Ca), we performed a Monte Carlo simulation. In short, the
179 correlation coefficients between randomly drawn single-spot Mg concentration, divided by measured
180 Ca, and measured Na/Ca_{cc} concentrations were compared to the correlation coefficient of measured
181 Na/Ca_{cc} and Mg/Ca_{cc} concentration ratios in our dataset. By using a Kernel fit of the measured data set
182 to draw the random data set and using the measured Ca as a common denominator we effectively
183 simulate the spurious correlation. The Monte Carlo results show that inter-element correlations are not
184 spurious, since the measured correlation coefficient is significantly higher than the distribution of the
185 correlation coefficients between 10.000 randomly drawn El¹ concentrations/measured Ca concentration
186 and measured El²/Ca concentrations (Appendix B).

187 Furthermore, to test whether Sr/Ca_{cc} and Na/Ca_{cc} variability in *A. lessonii* is not caused by variability in
188 Mg content due to a potential closed sum effect (since high amounts of incorporated Mg cations could
189 reduce the Ca content of the shell and hence result in apparently elevated Sr/Ca_{cc} and Na/Ca_{cc}), we
190 calculated maximum variability due to the sole effect of Mg-substitution. For *A. lessonii*, variability
191 (standard deviation) of ±0.09 mmol/mol in Na/Ca_{cc} and ±0.016 mmol/mol in Sr/Ca_{cc} around the mean
192 could be caused by variability in Mg/Ca_{cc} (assuming Mg substitutes for Ca in the calcite lattice, and Mg
193 plus Ca approximates 1 mol per mol calcite). This may have influenced the Sr/Ca_{cc} and Na/Ca_{cc}
194 regression slopes over salinity and also the calculated inter-element correlation coefficients, but only
195 by a maximum of ±1% for both elements, which is considerably lower than the total observed
196 variability within the dataset of 16% and 9%, respectively.

197 **2.3 Electron Microprobe Mapping**

198 To investigate variation of element distribution across the chamber wall, a number of cultured
199 specimens were prepared for Electron Microprobe Analysis (EPMA). From each of the five salinity
200 conditions, six specimens from both species were selected and embedded in resin (Araldite 2020) in an
201 aluminum ring (diameter 1 cm) in a vacuum chamber. Samples were polished with a final polishing
202 step using a diamond emulsion with grains of 0.04 µm. This procedure resulted in exposure of a cross-
203 section of the foraminiferal chamber wall from which areas for EPMA mapping were selected
204 (Appendix A). These areas were selected for being perpendicular to the shell outer surface, resulting in
205 pores completely crossing the exposed chamber wall. Elemental distributions were mapped in
206 chambers prior to F-3 to study the element distribution across the various layers of calcite (lamella)
207 produced with the addition of each new chamber in rotaliid foraminifera (Reiss, 1957, 1960).
208 Elemental distribution in the shell wall was measured using a field emission Electron Probe Micro
209 Analyser (JEOL JXA-8530F HyperProbe) at 7.0kV with a dwell time of 350 ms, using a spot diameter
210 of 80 nm and a step size between 0.1538 µm and 0.4072 µm (130 x 130 pixels).

211 Spatial resolution of the EPMA mapping was determined using the software package CASINO (monte
212 Carlo Simulation of electroN trajectory in SOLids, v 2.48). With the input parameters identical as used
213 in our analysis (80 nm spot size, beam current 7 KeV, etc.), the simulated surface radius of the
214 backscattered electrons (i.e. the spatial resolution) equals 590 nm. Semi-quantitative El/Ca_{cc} profiles

215 were calculated by averaging the $\text{El}/\text{Ca}_{\text{cc}}$ intensities parallel to the banding direction and applying a
216 constant calibration factor obtained from LA-ICP-MS measurements on the same specimen, similar to
217 the procedure of Egginis et al. (2004). We did not use the depth-resolved laser ablation-profiles for this
218 purpose, but used the average value from the profiles for correlation to the EPMA-derived intensities.

219 3. Results

220 3.1 Foraminiferal calcite element ratios and partitioning coefficients as a function of salinity

221 Per treatment, from lowest to highest salinity, average $\text{Na}/\text{Ca}_{\text{cc}}$ of the newly formed calcite varied
222 between 9.3 and 10.8 mmol/mol for *A. lessonii* and between 4.7 and 6.4 mmol/mol (highest salinity)
223 for *A. tepida* (Fig. 1), with a corresponding partition coefficient (note that partition coefficients are
224 'apparent', not taking into account speciation/activity of Na) ranging from 1.90×10^{-4} to 2.20×10^{-4} and
225 from 0.97×10^{-4} to 1.30×10^{-4} for *Amphistegina* and *Ammonia*, respectively (Table 3). For both
226 species, sets of single-specimen $\text{Na}/\text{Ca}_{\text{cc}}$ show slightly skewed distributions towards higher $\text{Na}/\text{Ca}_{\text{cc}}$ for
227 all salinities (Kolmogorov-Smirnov test, at the 95% confidence level). Combining all specimens (based
228 on the average of single-spot measurements per specimen), $\text{Na}/\text{Ca}_{\text{cc}}$ shows a positive linear relationship
229 with salinity for both *A. lessonii* and *A. tepida* ($\text{Na}/\text{Ca}_{\text{cc}} = 0.077 \pm 0.017 \times S + 7.13 \pm 0.60$, $F_{1,186} = 20.9$,
230 $p < 0.001$ for *A. lessonii* and $\text{Na}/\text{Ca}_{\text{cc}} = 0.064 \pm 0.013 \times S + 3.29 \pm 0.44$, $F_{1,172} = 25.9$, $p < 0.001$ for *A.*
231 *tepida*; Fig. 1). The observed average relative standard deviation between specimens in $\text{Na}/\text{Ca}_{\text{cc}}$ at each
232 of the 5 salinities is 15% for *A. lessonii* and 20% for *A. tepida*. The variance in $\text{Na}/\text{Ca}_{\text{cc}}$ between
233 individual specimens explained by salinity is $\eta^2 = 0.08$ for *A. lessonii* and $\eta^2 = 0.14$ for *A. tepida*.

234 Specimen's average $\text{Mg}/\text{Ca}_{\text{cc}}$ and $\text{Sr}/\text{Ca}_{\text{cc}}$ correlate positively with salinity in *A. tepida* ($\text{Mg}/\text{Ca}_{\text{cc}} =$
235 $0.060 \pm 0.011 \times S + 0.51 \pm 0.38$, $F_{1,172} = 29.9$, $p < 0.001$ and $\text{Sr}/\text{Ca}_{\text{cc}} = 0.014 \pm 12 \times 10^{-4} \times S + 1.00 \pm$
236 0.04 , $F_{1,337} = 254$, $p < 0.001$), whereas neither ratio correlates with salinity in *A. lessonii*. Average
237 relative standard deviations for the 5 salinity conditions per element are 27% for $\text{Mg}/\text{Ca}_{\text{cc}}$ and 9% for
238 $\text{Sr}/\text{Ca}_{\text{cc}}$ in *A. lessonii* and 32% in $\text{Mg}/\text{Ca}_{\text{cc}}$ and 7% for $\text{Sr}/\text{Ca}_{\text{cc}}$ for *A. tepida*. In *A. lessonii*, the
239 proportion of variance in $\text{Sr}/\text{Ca}_{\text{cc}}$ explained by salinity is $\eta^2 = 0.04$ ($p < 0.01$) ($\text{Mg}/\text{Ca}_{\text{cc}}$ not significant)
240 and for *A. tepida*, the proportion of variance in $\text{Sr}/\text{Ca}_{\text{cc}}$ explained by salinity is $\eta^2 = 0.44$ and in $\text{Mg}/\text{Ca}_{\text{cc}}$
241 $\eta^2 = 0.19$ ($p < 0.001$).

242 Single-spot analyses on *Ammonia tepida* show that $\text{Na}/\text{Ca}_{\text{cc}}$ and $\text{Mg}/\text{Ca}_{\text{cc}}$ are significantly correlated
243 within the salinity treatments, except for condition $S=30$ (Fig. 2). For the individual salinity treatments,
244 single-spot $\text{Sr}/\text{Ca}_{\text{cc}}$ and $\text{Mg}/\text{Ca}_{\text{cc}}$, as well as $\text{Na}/\text{Ca}_{\text{cc}}$ and $\text{Sr}/\text{Ca}_{\text{cc}}$ are not correlated significantly with
245 each other, except for $S=25$. Between salinity treatments, distributions in this species shift towards
246 higher $\text{Na}/\text{Ca}_{\text{cc}}$, $\text{Sr}/\text{Ca}_{\text{cc}}$ and $\text{Mg}/\text{Ca}_{\text{cc}}$ values with increasing salinity, although for the range between 30-
247 40 $\text{Na}/\text{Ca}_{\text{cc}}$ distributions remain rather similar (Fig. 2). For *Amphistegina lessonii*, distributions of
248 $\text{Sr}/\text{Ca}_{\text{cc}}$ and $\text{Mg}/\text{Ca}_{\text{cc}}$ ratios overlap largely between salinities, and only $\text{Na}/\text{Ca}_{\text{cc}}$ distributions shift
249 towards higher values (Fig. 2). Within each salinity condition however, single-spot $\text{Na}/\text{Ca}_{\text{cc}}$, $\text{Mg}/\text{Ca}_{\text{cc}}$
250 and $\text{Sr}/\text{Ca}_{\text{cc}}$ in this species are positively correlated amongst each other, whereby the $\text{Na}/\text{Ca}_{\text{cc}}$ intercept
251 of these relationships increases with increasing salinity (Fig. 2 and Appendix C).

252 **Table 3.** Average $\text{El}/\text{Ca}_{\text{cc}}$ ratios of the foraminiferal calcite (based on average of average specimens
 253 value per salinity (Sal) condition (S25-S45)) \pm standard error and corresponding apparent partitioning
 254 coefficients, defined as $D_{\text{El}} = (\text{El}/\text{Ca}_{\text{cc}})/(\text{El}/\text{Ca}_{\text{Seawater}})$ for *A. lessonii* (*A.l.*) and *A. tepida* (*A.t.*). 'n/spots'
 255 stands for number of specimens and average number of spots per specimen.

Sal	n/spots	Na/Ca _{cc} mmol/mol	D _{Na}	Mg/Ca _{cc} mmol/mol	D _{Mg}	Sr/Ca _{cc} mmol/mol	D _{Sr}
<i>A.l.</i>							
S25	65/2.6	9.29 \pm 0.27	1.90 $\times 10^{-4}$	33.35 \pm 1.20	5.94 $\times 10^{-3}$	1.80 \pm 0.026	0.199
S30	74/1.9	9.47 \pm 0.21	1.90 $\times 10^{-4}$	32.10 \pm 1.20	5.64 $\times 10^{-3}$	1.74 \pm 0.020	0.189
S35	103/1.9	9.63 \pm 0.18	1.98 $\times 10^{-4}$	32.71 \pm 1.07	5.94 $\times 10^{-3}$	1.76 \pm 0.018	0.191
S40	50/2	10.25 \pm 0.31	2.11 $\times 10^{-4}$	35.22 \pm 2.60	6.27 $\times 10^{-3}$	1.74 \pm 0.034	0.184
S45	44/1.4	10.78 \pm 0.30	2.20 $\times 10^{-4}$	33.80 \pm 1.68	5.90 $\times 10^{-3}$	1.82 \pm 0.036	0.189
<i>A.t.</i>							
S25	109/2.5	4.75 \pm 0.11	0.97 $\times 10^{-4}$	1.90 \pm 0.06	3.40 $\times 10^{-4}$	1.34 \pm 0.016	0.148
S30	58/1.8	5.63 \pm 0.22	1.13 $\times 10^{-4}$	2.41 \pm 0.09	4.24 $\times 10^{-4}$	1.44 \pm 0.013	0.156
S35	59/1.8	5.58 \pm 0.19	1.15 $\times 10^{-4}$	2.85 \pm 0.24	5.17 $\times 10^{-4}$	1.50 \pm 0.012	0.163
S40	93/1.8	5.70 \pm 0.16	1.17 $\times 10^{-4}$	2.73 \pm 0.15	4.86 $\times 10^{-4}$	1.55 \pm 0.017	0.164
S45	201.3	6.39 \pm 0.37	1.31 $\times 10^{-4}$	3.27 \pm 0.27	5.70 $\times 10^{-4}$	1.61 \pm 0.038	0.168

256

257 3.2 Size and chamber effect on Na/Ca_{cc} and inter-specimen variance

258 Specimens of *A. lessonii* produced most new chambers at salinities of 25, 30 and 35, closest to the
 259 salinity in their “natural” habitat (Burgers Zoo aquarium, salinity (33.9-34.3; Ernst et al., 2011). Size
 260 averages are not significantly different between these salinity treatments, based on a Kruskal-Wallis
 261 test, whereas specimens grown at salinities 40 and 45 were significantly smaller than those from lower
 262 salinities, reflecting lower chamber addition rates over the course of the culturing experiment at higher
 263 salinity (Fig. 3). Combining all specimens, Na/Ca_{cc} is not significantly related to size in *A. lessonii*.
 264 Specimens of *A. tepida* produced less chambers at salinity 45, possibly because such a high salinity is
 265 probably close to its tolerance levels (Murray, 2014), even though this species is adapted to relatively
 266 large salinity shifts in their tidal flat habitat. Specimens in the lower salinity groups (25, 30, 35) grew
 267 larger compared to specimens grown at two the highest salinity groups (Fig. 3). Combining all
 268 specimens, Na/Ca_{cc} is significantly related to size in *A. tepida*, yet with a small slope (-0.003) and just
 269 within the 95% confidence interval (p= 0.04).

270 Within each salinity tested, single-chambered Na/Ca_{cc} is slightly positively related to size for the
 271 specimens of *A. lessonii* cultured at salinities 25 (slope = 0.008, R² = 0.32, p < 0.01), 30 (slope = 0.002,
 272 R² = 0.11, p < 0.05 and 35 (slope = 0.005, R² = 0.18, p < 0.001). For the same species, Mg/Ca_{cc} is
 273 positively correlated to size at salinities 25, 30 and 35, with a similar slope of 0.03 (p < 0.05). Sr/Ca_{cc}
 274 also shows a positive relationship to size within salinities 25, 30 and 35 with slopes of 0.0007, 0.0003,
 275 0.0005 (p < 0.001) respectively. For *A. tepida*, there is only a slight negative correlation between size
 276 and Sr/Ca_{cc} for specimens cultured at salinity 25 (slope = 9.9 $\times 10^{-4}$, p < 0.001) and no significant
 277 correlation for the other conditions, or between size and Na/Ca_{cc} and Mg/Ca_{cc} in any of the salinities.

278 At the lowest salinity, Na/Ca_{cc} in the F-chamber (newest chamber) show slight (0.9 mmol/mol Na/Ca
 279 higher median) but significant higher values than the F-2 chambers for *A. lessonii* (multicompare test
 280 based on Kruskal-Wallis test, p < 0.05). For specimens of *A. lessonii* cultured at other salinities and for

281 *A. tepida* at any of the salinities tested, there no significant correlations between Na/Ca_{cc} and chamber
282 position were observed (note that only chamber positions F to F-2 were taken into account, as for the
283 lower chamber position sample numbers were insufficient). Furthermore, chamber position shows no
284 significant effect on Mg/Ca_{cc} and Sr/Ca_{cc}.

285 To further investigate the variance between and within individuals, a multiway ANOVA was
286 performed to investigate the effect on Na/Ca_{cc} per salinity condition. Inter-individual variance is
287 significant and larger than the variance between chamber groups and intra-individual variance in all
288 salinity groups, with the between individual variability accounting for $\eta^2 = 0.75 \pm 0.11 / 0.84 \pm 0.03$ of
289 the variance ($p < 0.001$) for *A. lessonii* and *A. tepida*, respectively. The variance due to chamber
290 position is not significant and the remaining intra-individual variance accounts for $\eta^2 = 0.09 \pm 0.05 /$
291 0.08 ± 0.05 for *A. lessonii* and *A. tepida*, respectively.

292 3.3 Elemental distributions in the chamber wall

293 EPMA maps of cross-sectioned chamber walls of *A. lessonii* show that, within the resolution limits of
294 the technique, bands of elevated Na/Ca_{cc} intensities overlap with zones of elevated Mg/Ca_{cc} (Fig. 4 and
295 appendix D). Mg bands show higher amplitudes than Na bands, but clearly coincide spatially.
296 Comparing EPMA maps with the backscatter SEM image of the exposed sections shows that the bands
297 with the highest Na/Ca_{cc} and Mg/Ca_{cc} occur in the proximity of the organic linings, which are clearly
298 visible in the backscatter SEM image (Fig. 4), with a number of high Na- and Mg-rich bands with
299 slightly lower maximum intensities occurring towards the outer chamber surface coinciding with
300 subsequent organic linings. For *A. tepida*, one band of elevated Mg/Ca_{cc} band is visible coinciding with
301 the POS with no clear Na/Ca_{cc} banding being detected.

302 4. Discussion

303 4.1 The effect of salinity and DIC on Na/Ca_{cc}, Mg/Ca_{cc} and Sr/Ca_{cc}

304 The single-specimen Na/Ca_{cc} data of the cultured *A. lessonii* and *A. tepida* both correlate positively
305 with salinity (Table 3, Fig. 1). This is in line with previous calibrations (for *Ammonia tepida*, Wit et al.,
306 2013; for cultured *Globigerinoides ruber*, Allen et al., 2016; for field-collected *G. ruber* and *G.*
307 *sacculifer*, Mezger et al., 2016). However, our Na/Ca-salinity calibration for *A. tepida* is somewhat less
308 sensitive than that observed earlier for the same species (Wit et al., 2013). An offset in Na/Ca_{cc} values
309 between calibrations for a single species has been reported previously for the planktonic *G. ruber* and
310 *G. sacculifer* (e.g. Mezger et al., 2016; Allen et al., 2016). Such an apparent discrepancy between
311 studies may be caused by differences between cultures or in situ conditions in one of the conditions not
312 focussed on (e.g. carbon chemistry, light intensity). Alternatively, subtle analytical differences (e.g.
313 differences in cleaning procedures), statistical reasons (for example differences in the number of
314 analyses or sample size) or the effect of genotypic variability on element incorporation (Sadekov et al.,
315 2016) may also play a role. Although the calibration presented here consists of many more data points
316 compared to those in Wit et al. (2013), we do not want to dismiss the latter as several parameters (like

317 cleaning procedures or the source of the seawater used for the culture media) inherently vary
318 (marginally) between studies. As such the difference observed between studies merely illustrates the
319 potential range for this species.

320 Contrasts in sensitivities such as observed for Na/Ca_{cc} between calibrations also apply to Mg/Ca_{cc} and
321 Sr/Ca_{cc}, both of which here show an increase with salinity in *A. tepida* but not in *A. lessonii* (Fig. 1).
322 Previous culturing experiments with *Ammonia tepida*, however, showed a smaller sensitivity of
323 Mg/Ca_{cc} to salinity (0.029-0.0044 mmol/mol change per salinity unit; Dissard et al., 2010b) than that
324 reported here (0.06). Still, all these sensitivities are considerably lower than that reported in Kısakürek
325 et al. (2008) for the planktonic *G. ruber* (0.23 when Mg/Ca_{cc} is assumed to increase linearly with
326 salinity), but in the same range as that reported by Nürnberg et al. (1996) for *G. sacculifer* (0.05). The
327 sensitivity of Sr/Ca_{cc} to salinity in *A. tepida* (0.014; Table 3) is comparable to that for *O. universa*
328 (0.008; Lea et al., 2008), *G. ruber* (0.02; Kısakürek et al., 2008) and similar to the significant effect of
329 salinity on Sr incorporation in the same species (0.01-0.02, depending on temperature) found by
330 Dissard et al. (2010b).

331 Sea water carbonate chemistry is an additional factor potentially affecting trace metal uptake (e.g. Lea
332 et al., 1999; Keul et al., 2017; Russell et al., 2004). Since salinity and dissolved inorganic carbon
333 concentration in the culture media co-varied in our experiments similar to the natural environment
334 (Table 1), Na/Ca_{cc} in our cultured specimens also correlates positively to sea water [DIC]. However,
335 sodium incorporation has been shown to be independent from changes in carbonate chemistry in
336 cultured *Amphistegina gibbosa* and several other benthic hyaline and porcelaneous species (Van Dijk et
337 al., 2017a). Additionally, Allen et al., (2016) also found no significant effect of carbonate chemistry
338 (i.e. varying [CO₃²⁻]) on Na incorporation in cultured *G. ruber*, suggesting that the variability in
339 Na/Ca_{cc} observed here in *A. lessonii* can be attributed to changes in salinity rather than [DIC].
340 However, future studies should disentangle the impacts of DIC and salinity on Na/Ca, in order to
341 increase proxy confidence in areas where Na/Ca and DIC relationships differ from the global average.
342 Previous studies showed that Sr/Ca_{cc} correlates positively to [DIC] in *A. tepida* (Keul et al., 2017),
343 which may account for part of the correlation between Sr/Ca_{cc} and salinity reported here for this
344 species. The published sensitivity of Sr/Ca_{cc} to [DIC] is approximately 2×10⁻⁵ mmol/mol change in
345 Sr/Ca_{cc} for every 1 μmol/kg change in [DIC], likely representing the maximum potential effect of DIC
346 on Sr partitioning given that others found no significant effect (Dissard et al., 2010a). For a change in
347 ~850 μmol/kg (Table 1), this would amount to an increase in Sr/Ca_{cc} of 0.019 mmol/mol (Keul et al.,
348 2017) over the salinity range studied here, thereby accounting for approximately 7% of the total
349 observed change in Sr/Ca_{cc} (Table 3). Inorganic carbon chemistry is known to affect growth rates and
350 shell weights in benthic foraminifera (Dissard et al., 2010a; Keul et al., 2013), which in turn, may
351 affect incorporation of Sr and Mg, hence providing a mechanistic link between inorganic carbon
352 chemistry and element partitioning.

353 El/Ca ratios of specimens of both species grown within each salinity condition are characterized by a
354 relatively large variability. In the overall data set, salinity only explains around 8% of the variation in
355 Na incorporation for *A. lessonii* and 14%, 19% and 44% of Na, Mg and Sr incorporation in *A. tepida*.
356 Nevertheless, for *A. lessonii*, the Na/Ca mean values (which translates to the values obtained from

357 traditional solution-ICP-MS) fit the regression model relatively well (Fig. 1). However, given the low
358 sensitivity, many specimens are required to reduce the uncertainty (Appendix E). This is reflected by
359 the relatively wide prediction bounds for the Na/Ca-salinity regressions, indicating an uncertainty
360 associated with a single Na/Ca_{cc} measurement. The relatively large inter-specimen variability in
361 element/Ca_{cc} ratios has been reported and discussed before (e.g. Sadekov et al., 2008; De Nooijer et al.,
362 2014a), but the cause for this variability remains to be identified.

363 **4.2 Inter-specimen, inter-species and intra-shell El/Ca_{cc} variability**

364 Single-chamber measurements show that Na/Ca_{cc} for both species varies between chambers (i.e.
365 specimens) with a RSD (Relative Standard Deviation) of 15%-20%, despite identical culture conditions
366 (Fig. 1). Since the analytical error on Na/Ca_{cc} accounts for approximately 2% (Table 2), a large portion
367 of the observed variability between specimens must be due to ontogeny and/or inter-specimen
368 differences in biomineralization controls (De Nooijer et al., 2014a).

369 Foraminiferal shell size at salinities 40 and 45 are significantly smaller than those cultured at lower
370 salinities. When combining data from all salinities, however, there is no (*A. lessonii*) or only a very
371 small (*A. tepida*) negative correlation between Na/Ca_{cc} and shell size, as opposed to a more substantial
372 negative correlation as observed by Wit et al. (2013). In fact, there appears to be a growth optimum
373 around salinity 30-35, whereas growth at higher salinities might be hampered (Fig. 3). This may
374 indicate that the earlier observed negative correlation between size and Na/Ca was the result of indirect
375 co-variation with salinity rather than a causal relationship resulting in lower Na/Ca values in smaller
376 specimens. This is corroborated by our observation that, for individuals grown at a similar salinity, the
377 relationship between Na/Ca_{cc} and size is either slightly positive or absent. Hence, size unlikely affects
378 the observed inter-specimen variability in Na/Ca_{cc}, which is supported by the absence of a correlation
379 between chamber position (and hence ontogenetic stage) and Na/Ca_{cc}. This implies that measuring
380 specimens of different size fractions or measuring different or multiple chambers should not
381 significantly affect the application of the Na/Ca_{cc} salinity proxy. However, sufficient specimens (n>30,
382 for an error margin <5% at the 95% confidence level; Sadekov et al., 2008; De Nooijer et al., 2014a)
383 are required for measurements. As most variability is between individuals rather than between
384 chambers (section 3.3), analyzing more chambers of the same specimen would increase the accuracy of
385 the measurement, but not improve the precision of the salinity estimate, given the large inter-specimen
386 variability. Without a major effect of ontogeny, physiological processes at the organismal level are
387 more likely to cause observed large inter-specimen variability in Na/Ca_{cc}, however these processes
388 remain poorly understood.

389 In *A. lessonii*, single-spot Na/Ca_{cc}, Sr/Ca_{cc} and Mg/Ca_{cc} are correlated amongst each other within each
390 salinity condition (Fig. 2). Correlation coefficients between the three element ratios are similar for the
391 different salinities, with superimposed an increase in the Na/Ca_{cc} relative to that of Mg/Ca_{cc} and Sr/Ca_{cc}
392 with increasing salinity (Appendix C). In contrast, single-spot Sr/Ca_{cc} and Mg/Ca_{cc} in *A. tepida* are not
393 correlated, whereas incorporation of all these elements increases significantly with salinity. Within
394 salinities Mg/Ca_{cc} and Na/Ca_{cc} are significantly correlated in 4 out of the 5 salinities, but with much
395 lower correlation coefficients compared to *A. lessonii* (Fig. 2 and Appendix C). However, between the

396 different salinities these elements are correlated in *A. tepida*, implying that for *A. tepida* salinity is one
397 of the actual parameters controlling Na/Ca_{cc}, Mg/Ca_{cc} and Sr/Ca_{cc} element uptake.

398 Within conditions, the correlations between both Sr/Ca_{cc} and Na/Ca_{cc} with Mg/Ca_{cc} in *A. lessonii* differ
399 from the correlation of Sr/Ca_{cc} with Mg/Ca_{cc} (correlation absent) and Na/Ca_{cc} with Sr/Ca_{cc} (weaker
400 correlation) for *A. tepida*. The differences between the correlations likely reflects differences in their
401 calcification pathway (e.g. transport of ions to the site of calcification) and/or might be explained by
402 differences in lattice strain due to the higher Mg-content in *A. lessonii*, whereas this effect is expected
403 to be less prominent in low-Mg species such as *A. tepida* (Evans et al., 2015). Differences in the
404 calcification pathway may also explain why Sr/Ca_{cc} and Mg/Ca_{cc} are correlated to salinity in *A. tepida*,
405 but not in *A. lessonii* (4.1).

406 In both species, Mg is found to be elevated in bands located close to the primary organic sheet and to
407 other organic layers (Fig. 4), present in rotaliid species due to their lamellar calcification mode (Reiss,
408 1957, 1960). This is similar to reports of within-chamber wall banding in many elements in other
409 species (Branson et al., 2016; Eggins et al., 2004; Sadekov et al., 2005; Paris et al., 2014; Spero et al.,
410 2015; Fehrenbacher et al., 2017; Kunioka et al., 2006; Steinhardt et al., 2015; Hathorne et al., 2009). In
411 planktonic species element banding has been related to diurnal light-dark cycles rather than the
412 addition of a new lamella with chamber addition (Spero et al., 2015; Fehrenbacher et al., 2017).
413 Whether in the species studied here, chamber addition (and hence element banding) is related to day
414 night cycles remains to be investigated. As in other studies, the Na- and Mg- bands are spatially
415 correlated (Fig. 4). For *Ammonia tepida*, the banding in both elements is less pronounced than for
416 *Amphistegina lessonii*, which is likely related to the (much) lower average Mg/Ca_{cc} and Na/Ca_{cc} ratios
417 in the former species. Alternatively, as the observations are close to the spatial resolution of the
418 method, the observed pattern could also be due to the band's width being smaller in *A. tepida* compared
419 to *A. lessonii*.

420 **4.3 Biomineralization controls on element uptake**

421 How elements are transported to the site of calcification and what is the role of sea water-vacuolization,
422 -leakage, trans-membrane-transport of ions, pH regulation and precipitation rate and how this differs
423 between species and specimens, remains to be discovered. The overall element composition of the
424 calcite precipitated by *A. lessonii* suggests that the calcification process of this species may more
425 closely resemble inorganic calcite precipitation from sea water, compared to that in *Ammonia tepida*
426 and other low-Mg calcite precipitating species. As a result, more elements (like Mg) are incorporated
427 and crystal lattice strain in intermediate-Mg calcite species is elevated, which may promote
428 incorporation of other elements through stress compensation (Mucci and Morse, 1983; Mewes et al.,
429 2015). This would explain the observed inter-element correlations within salinities. Another difference
430 between the species studied here may be caused by differences in CaCO₃ phase shifts during calcite
431 precipitation (e.g. Bots et al., 2012; De Yoreo et al., 2015). A metastable vaterite pre-cursor phase
432 recently found in two planktonic species may explain the low Mg incorporation relative to inorganic
433 calcite (Jacob et al., 2017). The higher Mg contents of *A. lessonii* could be related to the (partial)
434 absence of a vaterite-calcite transformation in this species. An Amorphous Calcium Carbonate (ACC)

435 pre-cursor phase has been observed in other marine biomineralising organisms (e.g. Weiner et al.,
436 2003; Giuffre et al., 2015) and often been hypothesised to play a role in foraminiferal calcification
437 (Erez, 2003; De Nooijer et al., 2014b), although it has not yet been directly detected. A higher Mg
438 concentration at the site of calcification could hypothetically result in a phase shift from amorphous
439 calcium carbonate (ACC) directly into calcite, whereby Mg is stabilizing the ACC, as described by
440 Littlewood et al. (2017). In inorganic calcite, the absence of a vaterite precursor phase also enhances
441 the incorporation of other metals incompatible to calcite, such as Sr (Littlewood et al., 2017) and a
442 similar process could hypothetically contribute to inter-species differences in element partitioning
443 similar to that observed here. Although the strong fractionation against Mg in *A. tepida* could reflect
444 double fractionation through a vaterite-calcite transformation (Jacob et al., 2017) the low-Mg content
445 might as well reflect a more enclosed site of calcification, whereby ions are mainly transported trans-
446 membrane (Nehrke et al., 2013; De Nooijer et al., 2014b). However, the experiments here do not allow
447 distinguishing between these (and other) potential mechanisms. Trans-membrane transport (TMT) of
448 Ca^{2+} and concomitant leakage of Mg^{2+} and Sr^{2+} might be more sensitive to differences in ionic strength
449 and element concentrations, hence possibly explaining the salinity effect on the incorporation of these
450 elements in *A. tepida* whereas it does not in *A. lessonii*, assuming that TMT relatively contributes more
451 to the supply of ions to the site of calcification in this species compared to *A. lessonii*, which might be
452 relatively more dependent on sea water vacuolisation. However, since there are many, both biotic and
453 abiotic, mechanisms that can (simultaneously) influence (coupled) element partitioning, it is
454 challenging to resolve the exact mechanism responsible for inter-specimen and inter-species
455 differences in El/Ca .

456 The spatial correlation between the intra-shell distributions of Mg and Na, associated to the organic
457 linings, suggests a coupled control on these elements during the calcification process, which is in line
458 with the observed inter-specimen correlations. This suggests that incorporation of these cations is
459 influenced by similar biomineralization mechanisms, related to sea water vacuolization (Erez, 2003;
460 Bentov and Erez, 2006), trans-membrane transport of elements (Nehrke et al., 2013), lattice-strain
461 effect (Evans et al., 2015) and/or metastable precursor phases (Jacob et al., 2017). The relative
462 contributions of these mechanisms might differ between species, resulting in the observed differences
463 in element incorporation and different inter-element correlations between species. Differences in the
464 efficiency of such processes between specimens might cause the observed inter-specimen variability,
465 whereas changes in these processes during the calcification time could be responsible for the observed
466 correlation between elements within the chamber wall.

467 **5. Conclusions**

468 By extending existing calibrations of the $\text{Na}/\text{Ca}_{\text{cc}}$ -salinity proxy to the intermediate-Mg calcite
469 precipitating benthic foraminifer *Amphistegina lessonii*, we show that the $\text{Na}/\text{Ca}_{\text{cc}}$ increase as a
470 function of salinity is similar to that in previously studied species. The absolute $\text{Na}/\text{Ca}_{\text{cc}}$ for *A. lessonii*
471 is, however, higher than that in *Ammonia tepida*. In *A. tepida*, $\text{Mg}/\text{Ca}_{\text{cc}}$ and $\text{Sr}/\text{Ca}_{\text{cc}}$ are positively
472 correlated to salinity, whereas they are not impacted by salinity in *A. lessonii*. Within each salinity,

473 single chamber-Na/Ca_{cc} and Mg/Ca_{cc} are positively correlated in *A. tepida*, whereas single chamber-
474 Sr/Ca_{cc} is not correlated to either Mg/Ca_{cc} or Na in this species. For *A. lessonii*, all Sr/Ca_{cc}, Mg/Ca_{cc} and
475 Na/Ca_{cc} combinations are positively correlated at the single chamber level. Electron Microprobe
476 Analysis mapping of Na and Mg within chamber walls of cultured specimens shows that in *A. lessonii*,
477 Na/Ca_{cc} and Mg/Ca_{cc} occur in elevated bands in close proximity to the primary organic lining. For
478 specimens of *A. tepida*, Mg-banding appears similar to that in *A. lessonii*, whereas Na-banding is less
479 prominent in this species. These results suggest that biomineralization controls on incorporated
480 elements differ between species.

481 **Author contributions**

482 GJ, LdN and EG designed the culture experiment and EG and IvD carried them out. EG and IvD
483 prepared the foraminiferal samples and analysed the specimens using EPMA. EG analysed the data and
484 prepared the manuscript with contributions from all co-authors.

485 **Acknowledgements**

486 We would like to thank Wim Boer for assistance with LA-ICP-MS measurements, Patrick Laan for sea
487 water measurements and Karel Bakker for DIC measurements. We kindly thank Max Janse (Burgers'
488 Zoo, Arnhem) for providing stock specimens of *A. lessonii* and Kirsten Kooijmans (NIOZ) for
489 providing cultures of *Dunaliella salina*. Sergei Matveev is thanked for assistance with the Electron
490 Microprobe analysis and Leonard Bik for assistance with polishing the samples. This work was carried
491 out under the program of the Netherlands Earth System Science Centre (NESSC), financially supported
492 by the Ministry of Education, Culture and Science (OCW) (Grantnr. 024.002.001) and Darwin Centre
493 for Biogeosciences (program 3020).

494 **References**

- 495 Allen, K. A., Hönisch, B., Eggins, S. M., Haynes, L. L., Rosenthal, Y., and Yu, J.: Trace element
496 proxies for surface ocean conditions: A synthesis of culture calibrations with planktic foraminifera,
497 *Geochimica et Cosmochimica Acta*, 193, 197-221, 2016.
- 498 Anand, P., Elderfield, H., and Conte, M. H.: Calibration of Mg/Ca thermometry in planktonic
499 foraminifera from a sediment trap time series, *Paleoceanography*, 18, 10.1029/2002kpa000846, 2003.
- 500 Barker, S., Greaves, M., and Elderfield, H.: A study of cleaning procedures used for foraminiferal
501 Mg/Ca paleothermometry, *Geochemistry, Geophysics, Geosystems*, 4, 2003.
- 502 Bemis, B. E., Spero, H. J., Bijma, J., and Lea, D. W.: Reevaluation of the oxygen isotopic composition
503 of planktonic foraminifera: Experimental results and revised paleotemperature equations,
504 *Paleoceanography*, 13, 150-160, 10.1029/98pa00070, 1998.
- 505 Bentov, S., and Erez, J.: Impact of biomineralization processes on the Mg content of foraminiferal
506 shells: A biological perspective, *Geochemistry Geophysics Geosystems*, 7, 10.1029/2005gc001015,
507 2006.
- 508 Bots, P., Benning, L. G., Rodriguez-Blanco, J.-D., Roncal-Herrero, T., and Shaw, S.: Mechanistic
509 insights into the crystallization of amorphous calcium carbonate (ACC), *Crystal Growth & Design*, 12,
510 3806-3814, 2012.
- 511 Branson, O., Bonnin, E. A., Perea, D. E., Spero, H. J., Zhu, Z., Winters, M., Hönisch, B., Russell, A.
512 D., Fehrenbacher, J. S., and Gagnon, A. C.: Nanometer-Scale Chemistry of a Calcite Biomineralization

513 Template: Implications for Skeletal Composition and Nucleation, Proceedings of the National
514 Academy of Sciences, 201522864, 2016.

515 De Nooijer, L. J., Hathorne, E. C., Reichart, G. J., Langer, G., and Bijma, J.: Variability in calcitic
516 Mg/Ca and Sr/Ca ratios in clones of the benthic foraminifer *Ammonia tepida*, Marine
517 Micropaleontology, 107, 32-43, 10.1016/j.marmicro.2014.02.002, 2014a.

518 De Nooijer, L. J., Spero, H. J., Erez, J., Bijma, J., and Reichart, G. J.: Biomineralization in perforate
519 foraminifera, Earth-Science Reviews, 135, 48-58, 10.1016/j.earscirev.2014.03.013, 2014b.

520 De Nooijer, L. J., Brombacher, A., Mewes, A., Langer, G., Nehrke, G., Bijma, J., and Reichart, G.-J.:
521 Ba incorporation in benthic foraminifera, Biogeosciences Discuss., 1-35, 2017.

522 De Yoreo, J. J., Gilbert, P. U., Sommerdijk, N. A., Penn, R. L., Whitlam, S., Joester, D., Zhang, H.,
523 Rimer, J. D., Navrotsky, A., and Banfield, J. F.: Crystallization by particle attachment in synthetic,
524 biogenic, and geologic environments, Science, 349, aaa6760, 2015.

525 Dickson, A., and Millero, F.: A comparison of the equilibrium constants for the dissociation of
526 carbonic acid in seawater media, Deep Sea Research Part A. Oceanographic Research Papers, 34,
527 1733-1743, 1987.

528 Dissard, D., Nehrke, G., Reichart, G.-J., and Bijma, J.: Impact of seawater $p\text{CO}_2$ on calcification and
529 Mg/Ca and Sr/Ca ratios in benthic foraminifera calcite: results from culturing experiments with
530 *Ammonia tepida*, Biogeosciences, 7, 81-93, 2010a.

531 Dissard, D., Nehrke, G., Reichart, G. J., and Bijma, J.: The impact of salinity on the Mg/Ca and Sr/Ca
532 ratio in the benthic foraminifera *Ammonia tepida*: Results from culture experiments, Geochimica Et
533 Cosmochimica Acta, 74, 928-940, 10.1016/j.gca.2009.10.040, 2010b.

534 Diz, P., Barras, C., Geslin, E., Reichart, G.-J., Metzger, E., Jorissen, F., and Bijma, J.: Incorporation of
535 Mg and Sr and oxygen and carbon stable isotope fractionation in cultured *Ammonia tepida*, Marine
536 Micropaleontology, 92, 16-28, 2012.

537 Dueñas-Bohórquez, A., Da Rocha, R. E., Kuroyanagi, A., De Nooijer, L. J., Bijma, J., and Reichart, G.
538 J.: Interindividual variability and ontogenetic effects on Mg and Sr incorporation in the planktonic
539 foraminifer *Globigerinoides sacculifer*, Geochimica Et Cosmochimica Acta, 75, 520-532,
540 10.1016/j.gca.2010.10.006, 2011.

541 Dueñas-Bohórquez, A., Da Rocha, R. E., Kuroyanagi, A., Bijma, J., and Reichart, G.-J.: Effect of
542 salinity and seawater calcite saturation state on Mg and Sr incorporation in cultured planktonic
543 foraminifera, Marine Micropaleontology, 73, 178-189, 2009.

544 Eggins, S. M., Sadekov, A., and De Deckker, P.: Modulation and daily banding of Mg/Ca in *Orbulina*
545 *universa* tests by symbiont photosynthesis and respiration: a complication for seawater thermometry?,
546 Earth and Planetary Science Letters, 225, 411-419, 10.1016/j.epsl.2004.06.019, 2004.

547 Elderfield, H., and Ganssen, G.: Past temperature and $\delta^{18}\text{O}$ of surface ocean waters inferred from
548 foraminiferal Mg/Ca ratios, Nature, 405, 442-445, 10.1038/35013033, 2000.

549 Erez, J.: The source of ions for biomineralization in foraminifera and their implications for
550 paleoceanographic proxies, Biomineralization, 54, 115-149, 10.2113/0540115, 2003.

551 Ernst, S., Janse, M., Renema, W., Kouwenhoven, T., Goudeau, M. L., and Reichart, G. J.: Benthic
552 foraminifera in a large indo-pacific coral reef aquarium, Journal of Foraminiferal Research, 41, 101-
553 113, 2011.

554 Evans, D., Erez, J., Oron, S., and Müller, W.: Mg/Ca-temperature and seawater-test chemistry
555 relationships in the shallow-dwelling large benthic foraminifera *Operculina ammonoides*, Geochimica
556 et Cosmochimica Acta, 148, 325-342, 2015.

557 Fehrenbacher, J. S., Russell, A. D., Davis, C. V., Gagnon, A. C., Spero, H. J., Cliff, J. B., Zhu, Z., and
558 Martin, P.: Link between light-triggered Mg-banding and chamber formation in the planktic
559 foraminifera *Neogloboquadrina dutertrei*, Pacific Northwest National Laboratory (PNNL), Richland,
560 WA (US), Environmental Molecular Sciences Laboratory (EMSL), 2017.

561 Giuffrè, A. J., Gagnon, A. C., De Yoreo, J. J., and Dove, P. M.: Isotopic tracer evidence for the
562 amorphous calcium carbonate to calcite transformation by dissolution–reprecipitation, Geochimica et
563 Cosmochimica Acta, 165, 407-417, 2015.

564 Guillong, M., Meier, D. L., Allan, M. M., Heinrich, C. A., and Yardley, B. W.: Appendix A6: SILLS:
565 A MATLAB-based program for the reduction of laser ablation ICP-MS data of homogeneous materials
566 and inclusions, Mineralogical Association of Canada Short Course, 40, 328-333, 2008.

567 Hathorne, E. C., James, R. H., Savage, P., and Alard, O.: Physical and chemical characteristics of
568 particles produced by laser ablation of biogenic calcium carbonate, Journal of Analytical Atomic
569 Spectrometry, 23, 240-243, 2008.

570 Hathorne, E. C., James, R. H., and Lampitt, R. S.: Environmental versus biomineralization controls on
571 the intratest variation in the trace element composition of the planktonic foraminifera *G. inflata* and *G.*
572 *scitula*, Paleoceanography, 24, 10.1029/2009pa001742, 2009.

573 Hayward, B. W., Holzmann, M., Grenfell, H. R., Pawlowski, J., and Triggs, C. M.: Morphological
574 distinction of molecular types in *Ammonia*—towards a taxonomic revision of the world's most
575 commonly misidentified foraminifera, *Marine Micropaleontology*, 50, 237-271, 2004.

576 Hönisch, B., Allen, K. A., Lea, D. W., Spero, H. J., Eggins, S. M., Arbuszewski, J., Rosenthal, Y.,
577 Russell, A. D., and Elderfield, H.: The influence of salinity on Mg/Ca in planktic foraminifers—
578 Evidence from cultures, core-top sediments and complementary $\delta^{18}\text{O}$, *Geochimica et Cosmochimica*
579 *Acta*, 121, 196-213, 2013.

580 Jacob, D., Wirth, R., Agbaje, O., Branson, O., and Eggins, S.: Planktic foraminifera form their shells
581 via metastable carbonate phases, *Nature Communications*, 8, 1265, 2017.

582 Keul, N., Langer, G., De Nooijer, L. J., and Bijma, J.: Effect of ocean acidification on the benthic
583 foraminifera *Ammonia* sp. is caused by a decrease in carbonate ion concentration, *Biogeosciences*, 10,
584 6185-6198, 2013.

585 Keul, N., Langer, G., Thoms, S., De Nooijer, L. J., Reichart, G.-J., and Bijma, J.: Exploring
586 foraminiferal Sr/Ca as a new carbonate system proxy, *Geochimica et Cosmochimica Acta*, 202, 374-
587 386, 2017.

588 Kısakürek, B., Eisenhauer, A., Böhm, F., Garbe-Schönberg, D., and Erez, J.: Controls on shell Mg/Ca
589 and Sr/Ca in cultured planktonic foraminiferan, *Globigerinoides ruber* (white), *Earth and Planetary*
590 *Science Letters*, 273, 260-269, 2008.

591 Kunioka, D., Shirai, K., Takahata, N., Sano, Y., Toyofuku, T., and Ujiie, Y.: Microdistribution of
592 Mg/Ca, Sr/Ca, and Ba/Ca ratios in *Pulleniatina obliquiloculata* test by using a NanoSIMS: Implication
593 for the vital effect mechanism, *Geochemistry Geophysics Geosystems*, 7, 10.1029/2006gc001280,
594 2006.

595 Lea, D. W., Mashiotta, T. A., and Spero, H. J.: Controls on magnesium and strontium uptake in
596 planktonic foraminifera determined by live culturing, *Geochimica Et Cosmochimica Acta*, 63, 2369-
597 2379, 10.1016/s0016-7037(99)00197-0, 1999.

598 Littlewood, J. L., Shaw, S., Peacock, C. L., Bots, P., Trivedi, D., and Burke, I. T.: Mechanism of
599 Enhanced Strontium Uptake into Calcite via an Amorphous Calcium Carbonate Crystallization
600 Pathway, *Crystal Growth & Design*, 17, 1214-1223, 2017.

601 Mehrbach, C., Culberson, C., Hawley, J., and Pytkowicz, R.: Measurement of the apparent dissociation
602 constants of carbonic acid in seawater at atmospheric pressure, *Limnology and Oceanography*, 18, 897-
603 907, 1973.

604 Mewes, A., Langer, G., De Nooijer, L. J., Bijma, J., and Reichart, G. J.: Effect of different seawater
605 Mg^{2+} concentrations on calcification in two benthic foraminifers, *Marine Micropaleontology*, 113, 56-
606 64, 10.1016/j.marmicro.2014.09.003, 2014.

607 Mewes, A., Langer, G., Reichart, G.-J., De Nooijer, L. J., Nehrke, G., and Bijma, J.: The impact of Mg
608 contents on Sr partitioning in benthic foraminifers, *Chemical Geology*, 412, 92-98, 2015.

609 Mezger, E., De Nooijer, L. J., Boer, W., Brummer, G., and Reichart, G. J.: Salinity controls on Na
610 incorporation in Red Sea planktonic foraminifera, *Paleoceanography*, 2016.

611 Mucci, A., and Morse, J. W.: The incorporation of Mg^{2+} and Sr^{2+} into calcite overgrowths: influences
612 of growth rate and solution composition, *Geochimica et Cosmochimica Acta*, 47, 217-233,
613 [http://dx.doi.org/10.1016/0016-7037\(83\)90135-7](http://dx.doi.org/10.1016/0016-7037(83)90135-7), 1983.

614 Murray, J. W.: *Ecology and palaeoecology of benthic foraminifera*, Routledge, 2014.

615 Nehrke, G., Keul, N., Langer, G., De Nooijer, L. J., Bijma, J., and Meibom, A.: A new model for
616 biomineralization and trace-element signatures of Foraminifera tests, *Biogeosciences*, 10, 6759-6767,
617 10.5194/bg-10-6759-2013, 2013.

618 Nürnberg, D., Bijma, J., and Hemleben, C.: Assessing the reliability of magnesium in foraminiferal
619 calcite as a proxy for water mass temperatures, *Geochimica et Cosmochimica Acta*, 60, 803-814, 1996.

620 Paris, G., Fehrenbacher, J. S., Sessions, A. L., Spero, H. J., and Adkins, J. F.: Experimental
621 determination of carbonate-associated sulfate delta S-34 in planktonic foraminifera shells,
622 *Geochemistry Geophysics Geosystems*, 15, 1452-1461, 10.1002/2014gc005295, 2014.

623 Raja, R., Saraswati, P. K., and Iwao, K.: A field- based study on variation in Mg/Ca and Sr/Ca in larger
624 benthic foraminifera, *Geochemistry, Geophysics, Geosystems*, 8, 2007.

625 Reichart, G. J., Jorissen, F., Anschutz, P., and Mason, P. R. D.: Single foraminiferal test chemistry
626 records the marine environment, *Geology*, 31, 355-358, 10.1130/0091-
627 7613(2003)031<0355:sfctct>2.0.co;2, 2003.

628 Reiss, Z.: The *Bilamellidea*, nov. superfam., and remarks on Cretaceous *globorotaliids*, *Contrib*
629 *Cushman Found Forum Res*, 8, 127-145, 1957.

630 Reiss, Z.: Structure of so-called Eponides and some other rotaliiform foraminifera, State of Israel,
631 Ministry of Development, Geological Survey, 1960.

632 Rohling, E., and Hilgen, F.: The eastern Mediterranean climate at times of sapropel formation: a
633 review, *Netherlands Journal of Geosciences/Geologie en Mijnbouw*, 2007.

634 Rosenthal, Y., Lohmann, G. P., Lohmann, K. C., and Sherrell, R. M.: Incorporation and preservation of
635 Mg in *Globigerinoides sacculifer*: Implications for reconstructing the temperature and $^{18}\text{O}/^{16}\text{O}$ of
636 seawater, *Paleoceanography*, 15, 135-145, 10.1029/1999pa000415, 2000.

637 Russell, A. D., Hönisch, B., Spero, H. J., and Lea, D. W.: Effects of seawater carbonate ion
638 concentration and temperature on shell U, Mg, and Sr in cultured planktonic foraminifera, *Geochimica
639 et Cosmochimica Acta*, 68, 4347-4361, 2004.

640 Sadekov, A., Eggins, S. M., De Deckker, P., and Kroon, D.: Uncertainties in seawater thermometry
641 deriving from intratest and intertest Mg/Ca variability in *Globigerinoides ruber*, *Paleoceanography*, 23,
642 10.1029/2007pa001452, 2008.

643 Sadekov, A. Y., Eggins, S. M., and De Deckker, P.: Characterization of Mg/Ca distributions in
644 planktonic foraminifera species by electron microprobe mapping, *Geochemistry Geophysics
645 Geosystems*, 6, 10.1029/2005gc000973, 2005.

646 Sadekov, A. Y., Darling, K. F., Ishimura, T., Wade, C. M., Kimoto, K., Singh, A. D., Anand, P.,
647 Kroon, D., Jung, S., and Ganssen, G.: Geochemical imprints of genotypic variants of *Globigerina
648 bulloides* in the Arabian Sea, *Paleoceanography*, 31, 1440-1452, 2016.

649 Segev, E., and Erez, J.: Effect of Mg/Ca ratio in seawater on shell composition in shallow benthic
650 foraminifera, *Geochemistry Geophysics Geosystems*, 7, 10.1029/2005gc000969, 2006.

651 Spero, H. J., Eggins, S. M., Russell, A. D., Vetter, L., Kilburn, M. R., and Hönisch, B.: Timing and
652 mechanism for intratest Mg/Ca variability in a living planktic foraminifer, *Earth and Planetary Science
653 Letters*, 409, 32-42, 10.1016/j.epsl.2014.10.030, 2015.

654 Steinhardt, J., De Nooijer, L. L., Brummer, G. J., and Reichert, G. J.: Profiling planktonic foraminiferal
655 crust formation, *Geochemistry, Geophysics, Geosystems*, 16, 2409-2430, 2015.

656 Stoll, M. H. C., Bakker, K., Nobbe, G. H., and Haese, R. R.: Continuous-flow analysis of dissolved
657 inorganic carbon content in seawater, *Analytical Chemistry*, 73, 4111-4116, 10.1021/ac010303r, 2001.

658 Terakado, Y., Ofuka, Y., and Tada, N.: Rare earth elements, Sr, Ba, Fe, and major cation
659 concentrations in some living foraminiferal tests collected from Iriomote Island, Japan: An exploration
660 for trace element behavior during biogenic calcium carbonate formation, *Geochemical Journal*, 44,
661 315-322, 2010.

662 Toyofuku, T., Kitazato, H., Kawahata, H., Tsuchiya, M., and Nohara, M.: Evaluation of Mg/Ca
663 thermometry in foraminifera: Comparison of experimental results and measurements in nature,
664 *Paleoceanography*, 15, 456-464, 10.1029/1999pa000460, 2000.

665 Toyofuku, T., Suzuki, M., Suga, H., Sakai, S., Suzuki, A., Ishikawa, T., De Nooijer, L. J., Schiebel, R.,
666 Kawahata, H., and Kitazato, H.: Mg/Ca and $\delta^{18}\text{O}$ in the brackish shallow-water benthic foraminifer
667 *Ammonia 'beccarii'*, *Marine Micropaleontology*, 78, 113-120, 2011.

668 Van Aken, H. M.: Variability of the water temperature in the western Wadden Sea on tidal to
669 centennial time scales, *Journal of Sea Research*, 60, 227-234, 2008.

670 Van Dijk, I., De Nooijer, L. J., and Reichert, G.-J.: Trends in element incorporation in hyaline and
671 porcelaneous foraminifera as a function of $p\text{CO}_2$, *Biogeosciences*, 14, 497, 2017a.

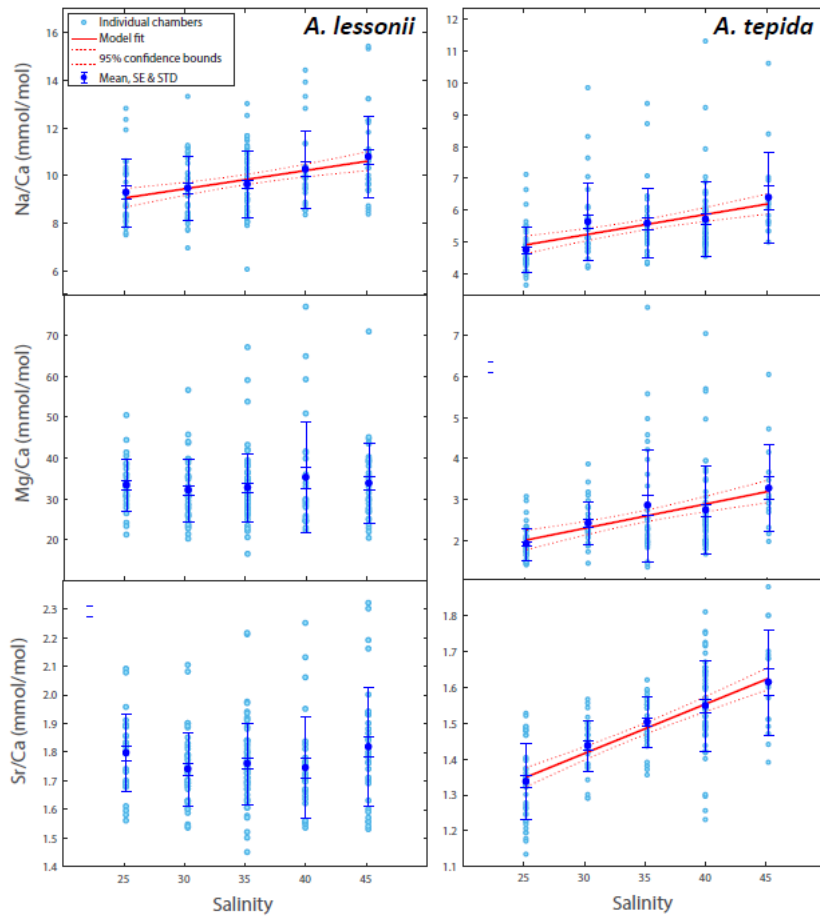
672 Van Dijk, I., De Nooijer, L. J., Wolthers, M., and Reichert, G.-J.: Impacts of pH and $[\text{CO}_3^{2-}]$ on the
673 incorporation of Zn in foraminiferal calcite, *Geochimica et Cosmochimica Acta*, 197, 263-277, 2017b.

674 Van Heuven, S., Pierrot, D., Rae, J., Lewis, E., and Wallace, D.: MATLAB program developed for
675 CO₂ system calculations, Oak Ridge, Tennessee: Carbon Dioxide Information Analysis Center, Oak
676 Ridge National Laboratory, US Department of Energy. pp. ORNL/CDIAC-105b, 2011.

677 Weiner, S., Levi-Kalishman, Y., Raz, S., and Addadi, L.: Biologically formed amorphous calcium
678 carbonate, *Connective Tissue Research*, 44, 214-218, 2003.

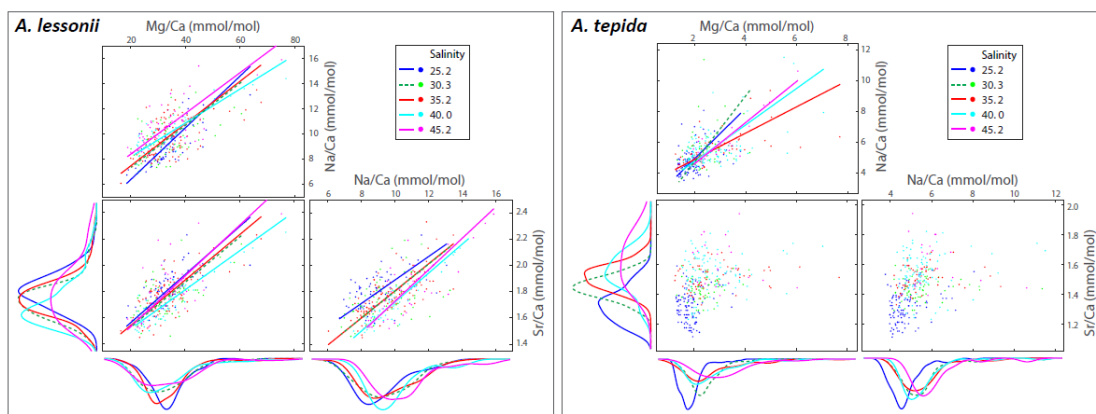
679 Wit, J. C., De Nooijer, L. J., Wolthers, M., and Reichert, G. J.: A novel salinity proxy based on Na
680 incorporation into foraminiferal calcite, *Biogeosciences*, 10, 6375-6387, 10.5194/bg-10-6375-2013,
681 2013.

682



683

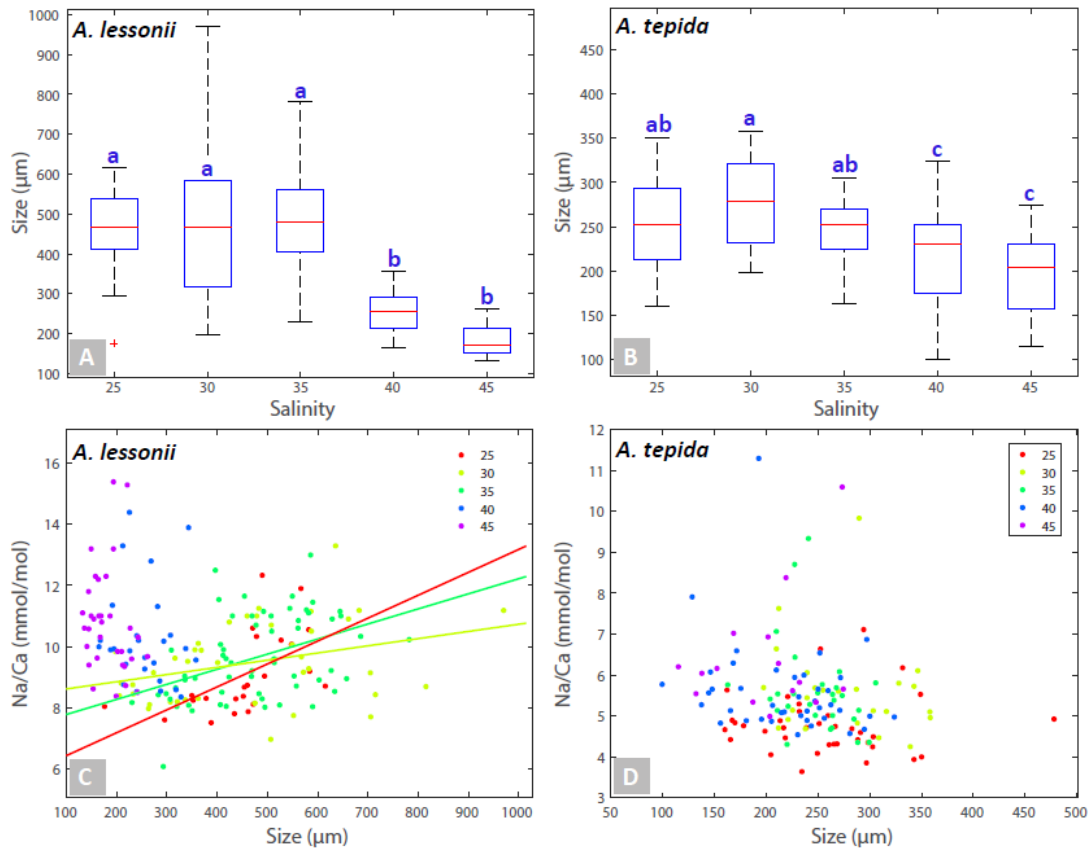
684 **Figure 1. Foraminiferal Na/Ca_{cc}, Mg/Ca_{cc} and Sr/Ca_{cc} versus salinity. Light blue dots represent the average**
 685 **per specimen (n= 359 for *A. lessonii*, n= 339 for *A. tepida*, with 2-3 measured chambers per individual), dark**
 686 **blue dots indicate the mean, with inner error bars indicating the standard error and outer error bars the**
 687 **standard deviation for each treatment. The linear regression model (red line) is based on the individuals'**
 688 **mean, with the 95% confidence interval of the regression in dashed lines.**



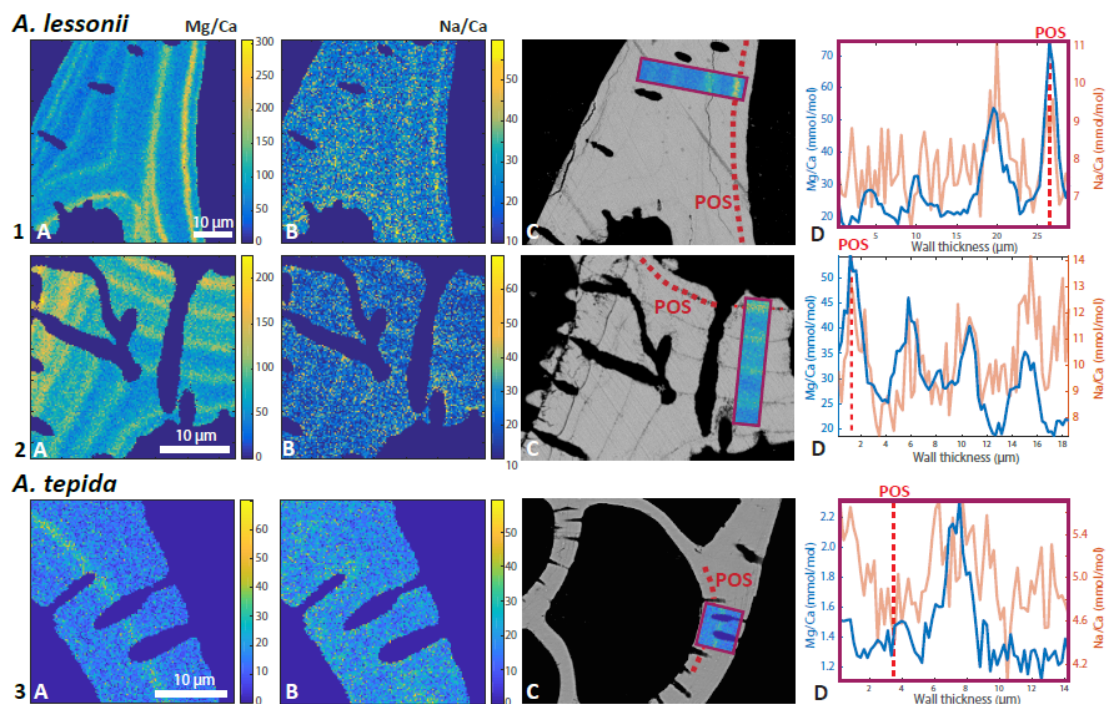
689

690 **Figure 2. Individual chamber LA-ICP-MS analyses showing correlations between foraminiferal Mg/Ca_{cc},**
 691 **Sr/Ca_{cc} and Na/Ca_{cc} for *A. tepida* (left) and *A. lessonii* (right) per salinity condition. Significant orthogonal**
 692 **linear regressions are indicated with a line, colour coded for salinity (see legend). Correlation coefficients,**
 693 **slope and intercepts of these regressions can be found in Appendix C. In short, within salinity conditions,**
 694 **element ratios are strongly correlated with each other in *A. lessonii*, whereas in *A. tepida*, element ratios do**

695 not (strongly) correlate with each other. When combining all single-spot data in *A. tepida*, element ratios
 696 correlate amongst each other because the incorporation of all three elements increases with salinity, shifting
 697 the distributions to higher values. In *A. lessonii*, only the Na/Ca_{cc} distributions shift towards higher values
 698 with increasing salinity, whereas Mg/Ca_{cc} and Sr/Ca_{cc} distributions are relatively similar between salinity
 699 conditions.



700
 701 **Figure 3.** Boxplots (Panel A and B) showing the size distributions (median, 1st and 3rd quartiles, minimum
 702 and maximum values) for each salinity condition, n= 24, 40, 60, 27, 33 for *A. lessonii* and n= 38, 24, 28, 41,
 703 15 for *A. tepida*. Letters (a, b, c) indicate significant different population means, based on ANOVA (p <
 704 0.001). Panel C and D show the Na/Ca values against size measurements per individual, colour coded per
 705 salinity condition (see legend), for *A. lessonii* and *A. tepida*. Significant linear regression lines are plotted for
 706 *A. lessonii*.



707
 708 **Figure 4.** Foraminiferal Mg/Ca_{cc} (A panels; left) and Na/Ca_{cc} (B panels) intensity ratio maps, obtained with
 709 EPMA, for two specimens of *A. lessonii* grown at a salinity of 30 (row 1) and 25 (row 2) and one specimen of
 710 *A. tepida* (row 3). D panels (right) show profiles for Mg/Ca (blue) and Na/Ca (red), based on averaged
 711 EPMA ratios scaled to LA-ICP-MS measurements of the same specimen, of an averaged lateral profile area
 712 through the chamber wall perpendicular to the lamella separated by organic linings (purple rectangles C).
 713 The transect area is indicated with a purple rectangle, on top of a backscatter SEM image (C), showing that
 714 the high EI/Ca bands overlap with the primary organic sheet (POS, marked with dashed red line) and
 715 subsequent organic linings. See Appendix D for the results for three more specimens.

716 **Appendix**

717 **Appendix A.**

718 SEM image of a specimen of *A. lessonii* showing LA-ICP-MS measurement spots (panel A) and SEM images
 719 of specimens of *A. lessonii* (panel B) and *A. tepida* (panel C) embedded in resin and polished for Electron
 720 Probe Micro Analysis, the mapping area is depicted with a white box.

721 **Appendix B.**

722 Results of the Monte Carlo analysis showing that the measured correlation coefficients for the inter-
 723 specimen correlations between the measured EI¹/Ca_{cc} and EI²/Ca_{cc} are not caused by a spurious correlation
 724 due to the common denominator Ca_{cc}, showing that the measured correlation coefficient is significantly
 725 higher than the distribution of the correlation coefficients between 10.000 randomly drawn EI¹
 726 concentrations/measured Ca concentration and measured EI²/Ca concentrations. This test is based on the
 727 concentration results from a single LA-ICP-MS session with specimens of *A. lessonii* cultured at a salinity of
 728 35.

729 **Appendix C.**

730 **Results for the orthogonal regressions testing the correlations between single-spot El^1/Ca and El^2/Ca , within**
731 **salinity conditions, for *A. lessonii* and *A. tepida*.**

732 **Appendix D.**

733 **Foraminiferal Mg/Ca_{cc} and Na/Ca_{cc} (A and B, E and F) intensity ratio maps, obtained with EPMA, for two**
734 **specimens of *A. lessonii* grown at a salinity of 30 (A-D) and 35 (E-H). Panel D and H show profiles for**
735 **Mg/Ca (blue) and Na/Ca (red), based on averaged EPMA ratios scaled to LA-ICP-MS measurements in D**
736 **and on EPMA count ratios in H (no La-ICP-MS data available for this specimen), of an averaged transect**
737 **area through the chamber wall perpendicular to the POS. The transect areas (purple rectangles) are**
738 **indicated on top of backscatter SEM images (C and G), showing that the high El/Ca bands overlap with the**
739 **primary organic sheet (POS, in dashed red line in C, not clear in G)) and subsequent organic linings.**

740 **Appendix E.**

741 **Figure showing the relationship between the salinity uncertainty and number of measured specimens for the**
742 **Na/Ca_{cc} - salinity calibration of *A. lessonii*, calculated following Eq. (1):**

743 **Salinity uncertainty = $(2 \times RSD \times \text{Number of specimens}^{-0.5}) / \text{Sensitivity}$,** (1)

744 **whereby sensitivity is the slope of the calibration.**